Digitally Mapping Gypsic and Natric Soil Areas Using Landsat ETM Data

S. J. Nield
USDA-NRCS
Federal Bldg.
P.O. Box 33124
100 East B St.
3rd Floor
Casper, WY 82602-5011

J. L. Boettinger*
Dep. of Plants, Soils, and Biometeorology
Utah State Univ.
4820 Old Main Hill
Logan, UT 84322-4820

R. D. Ramsey
Dep. of Wildland Resources
Utah State Univ.
5230 Old Main Hill
Logan, UT 84322-5230

Mapping salt-affected soils in remote rangelands is challenging. We used Landsat 7 ETM data to facilitate digital mapping of gypsic and natric soil areas in the upper Colorado River drainage. Optimum index factor band combinations were used to explore the scene. Normalized difference ratio models and threshold values were developed by comparing spectral signatures with gypsic and natric soil areas verified in the field. Gypsic soil areas were mapped using the normalized difference ratio of Bands 5 and 7 with a threshold >0.11, probably related to the spectral reflectance of gypsum within a few centimeters of the surface. All sites predicted to be gypsic soil areas were determined to be gypsic by field assessment, and 87% of the field-observed gypsic soil areas were correctly predicted. Natric soil areas were mapped using the normalized difference ratio of Bands 5 and 4 with a threshold >0.19, possibly related to the co-occurrence of Fe-bearing minerals with natric soil areas. Most of the sites predicted to be natric were determined in the field to be natric (82%), but only half of the field-observed natric areas were correctly predicted, indicating that natric soils are harder to detect spectrally than gypsic soils. While the gypsic model may be transferred to other areas, particularly in the arid Colorado Plateau, transfer of natric models would be difficult. Normalized difference ratio models can be developed for other digital soil mapping areas where land surface features produce differences in Landsat spectral band reflectances.

Abbreviations: DEM, digital elevation model; NDVI, normalized difference vegetation index; NIR, near infrared; OIF, optimum index factor; SWIR, shortwave infrared.

Assessing the distribution and extent of salt-affected soils in expansive, arid, rangeland areas is difficult. Such a landscape may be well suited for analysis with satellite-derived remotely sensed data because of low vegetation cover, thus the majority of its spectral response would be generated by soil and rock surface characteristics. Spectral characteristics of different land surfaces associated with distinct soil types and their mineral assemblages (e.g., Baumgardner et al., 1985; Ben-Dor, 2002; Brown et al., 2006) may provide a means of quickly and remotely identifying and delineating salt-affected soils.

Satellite-derived remote sensing uses space-borne sensor platforms to quantify the reflectance or emissions of electromagnetic radiation from the Earth (Lillesand and Kiefer, 2000). These reflectance and emission data can be analyzed to extract information about the Earth and its resources, and how the properties of different objects and surfaces vary across the electromagnetic spectrum. Satellite imagery can have a variety of spectral and spatial properties. Spectral resolution refers to the number of spectral bands used by a particular sensor and the width of the electromagnetic spectrum sensed in each band, whereas spatial resolution refers to the area on the ground represented by an individual pixel. Spectral bands with contrasting reflectance characteristics for a minimum area on a given surface can be compared to enhance those specific characteristics and differentiate features on the Earth's surface.

Soil Sci. Soc. Am. J. 71:245-252
doi:10.2136/sssaj2006-0049
Received 3 Feb. 2006.
*Corresponding author (janis.boettinger@usu.edu).

The National Aeronautics and Space Administration's Landsat satellite program has been used for many land surface applications (National Aeronautics and Space Administration, 2006), including mapping and monitoring vegetation in arid and semiarid regions (e.g., Ramsey et al., 2004; Clark et al., 2001). The most recent sensor, Landsat 7 Enhanced Thematic Mapper (ETM) (launched 15 Apr. 1999), which is similar in spectral and spatial resolution to the older but still commissioned Landsat 5 Thematic Mapper, has seven spectral bands that integrate specific wavelength segments of the electromagnetic spectrum with a minimum spatial resolution of 30 m in the visible (three bands), near-infrared (NIR, one band), shortwave infrared (SWIR, two bands), and thermal infrared (one band) (Table 1).

Many researchers have used Landsat data to map or characterize salt-affected soil surface features. Rao et al. (1995) used Landsat 5 Thematic Mapper data to characterize the spectral response of saline, saline–sodic, and sodic soils. They reported ≥10% more reflectance in the NIR band for saline, saline–sodic, and sodic soils than for normal soils. The high reflectance values of salt-affected soils in visible light and their lack of plant cover have been used to delineate or monitor changes in salt-affected soils (e.g., Pankova and Rukhovich, 1999; Dwivedi et al., 1999; Masoud and Koike, 2006). After stratifying their study area geomorphically, Metternicht and Zinck (1997) used supervised classification of Landsat 7 ETM data to map classes of salt- and Na-affected soil surfaces differentiated by geomorphology, soil pH, and electrical conductivity (EC) (overall classification accuracy of 64%). Fernandez-Buces et al. (2006) correlated EC and sodium adsorption ratio (SAR) of soil extracts with soil and halophytic plant spectral response measured with a field radiometer, and developed a combined spectral response index (CSRI) calculated from the normalized difference vegetation index (NDVI); the CSRI was extrapolated spatially using some Landsat ETM data to predict EC and SAR on the landscape. Because many

Table 1. Landsat 7 ETM spatial and spectral band resolutions. Bands 1 through 5 and 7 were used in this research.

Band	Spatial resolution	Spectral range	Common name†
	m	μm	
1	30	0.450–0.515	Blue
2	30	0.525–0.605	Green
3	30	0.630–0.690	Red
4	30	0.775–0.900	NIR
5	30	1.550–1.750	SWIR (MIR)
6	60	10.40–12.50	TIR
7	30	2.090–2.350	SWIR (MIR)
Pan	15	0.520–0.900	Visible + NIR

† NIR = near infrared; SWIR = shortwave infrared (formerly MIR = middle infrared, 1–3 μm; Lillesand and Kiefer, 2000); TIR = thermal infrared.

saline areas along the margins of playa lakes are temporally and spatially variable, Kienast-Brown and Boettinger (2006) used supervised classification of Landsat 7 ETM data to refine the mapping of saline and wet soils on the shore of the Great Salt Lake.

The upper San Rafael River, which cuts through the northwestern flank of the San Rafael Swell in central Utah, provides an ideal setting in which to digitally map salt-affected rangeland soils using Landsat data. The headwater area of the San Rafael River is a major contributor of total dissolved solids to the greater Colorado River basin (Utah Department of Environmental Quality, 2004), and mapping salt-affected soil could help target management of potential salinity sources. In this arid area, climate is relatively uniform and vegetation is sparse, and an eroded monocline exposes a diversity of sedimentary geologic formations that are the parent materials for gypsic and natric soils. We hypothesized that spectral properties of land surfaces associated with gypsic and natric soil areas could be quantified using satellite-derived remote sensing data and used to predict the occurrence of salt-affected soils on the landscape. To test this hypothesis, we analyzed Landsat 7 ETM data, developed normalized difference ratio models to spectrally classify gypsic and natric soils, and assessed the accuracy of the models in the field.

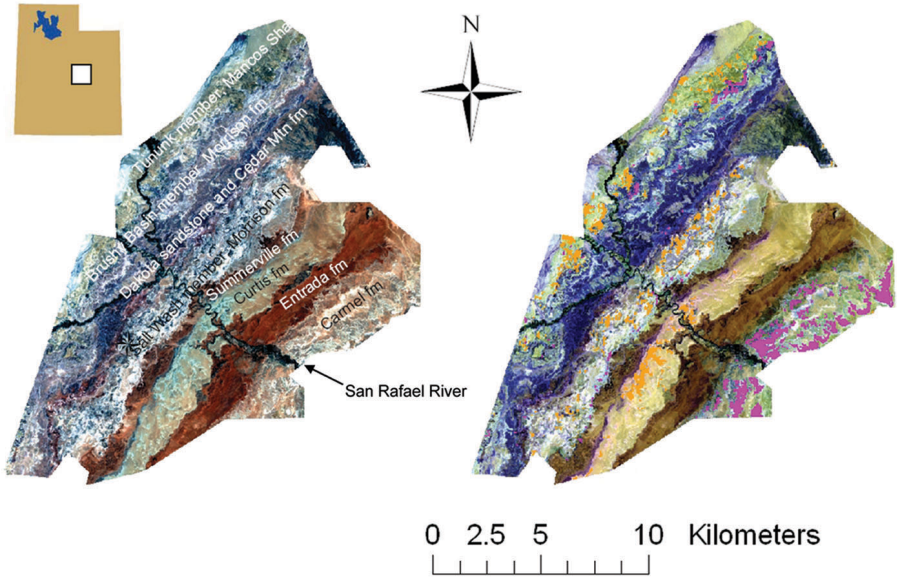

Fig. 1. Landsat 7 ETM images of 22 000-ha study area in the upper San Rafael River drainage in the northeastern San Rafael Swell, and location of the study area in central Utah (upper left inset). In the left-hand image, visible Landsat Bands 3, 2, and 1 are assigned to red, green, and blue, respectively, and geologic formations (fm) and the San Rafael River are labeled. In the right-hand image, Landsat Bands 7, 5, and 1 are assigned to red, green, and blue, respectively, showing the location of gypsic (magenta) and natric (orange) soil areas determined using the gypsic and natric index models.

MATERIALS AND METHODS

Study Area

A study area of 22 209 ha was delineated in the upper San Rafael River drainage in the northern part of the San Rafael Swell, about 48 km south of Price, UT, in the Colorado Plateau physiographic region (Fig. 1). The study area is roughly bisected by the upper San Rafael River, formed by the convergence of Ferron, Cottonwood, and Huntington creeks (Fig. 1).

The San Rafael Swell is a northeast- to southwest-trending monocline resulting from deformation of sedimentary strata overlying reverse faulting in the basement rocks (Fillmore, 2000). Jurassic (144–206 million yr) and Cretaceous (65–144 million yr) geologic formations reflecting oceanic transgressive and regressive cycles are exposed, increasing in age with elevation (1523–2132 m) from west to east (Fig. 1). Jurassic rocks include the Carmel (gypsum-rich mudstone and siltstone), Entrada (sandstone), Curtis (calcareous sandstone), and Summerville (siltstones and mudstones) formations, and the Salt Wash (conglomerate and sandstone) and Brushy Basin (mudstone) members of the Morrison formation. Cretaceous rocks include the Cedar Mountain (conglomerate and sandstone) and Dakota (sandstone) formations, and the Tununk (shale) member of the Mancos formation.

Mean annual precipitation is 13 to18 cm, mean annual air temperature is 7 to 10°C (estimated from climatic data for Castle Dale, UT, from the Western Regional Climate Center, www.wrcc.dri.edu/ [verified 14 Sept. 2006]), and average annual pan evaporation is 120 cm (from 1950–1980 data from Sunnyside, UT; Jensen and Borchert, 1988), indicating a warm, sunny climate of low humidity. Precipitation is fairly evenly distributed, but summer precipitation typically arrives as thunderstorms born of moisture-laden air from the Gulf of California and the Gulf of Mexico, which can deposit 2 cm of rain in ≤1 h and result in flash flooding. The soil temperature regime is mesic and the soil moisture regime is aridic.

The study area contains a wide variety of gypsic and natric soils, which appear closely tied to specific geologic formations. Gypsum-rich (gypsic) soils of the Mussentuchit (coarse-loamy, gypsic, mesic Typic Calcigypsids), Goblin (loamy, gypsic, mesic, shallow Typic Torriorthents), and Robroost (coarse-loamy, mixed, active, mesic Typic Calcigypsids) series occur in highly dissected terrain of the Carmel formation associated with gypsum-rich rock outcrops. Mussentuchit soils occur on shoulders and summits, Goblin soils occur on sideslopes, and Robroost soils occupy footslope and depressional areas. Gypsum concentration in the Mussentuchit and Goblin series soils can exceed 50% by weight in By and Cy horizons, which can occur within a few centimeters of the soil surface.

Sodium-rich (natric) soils of the Hadden (fine-loamy, mixed, superactive, mesic Typic Natrargids) and Bributte (clayey, smectitic, calcareous, mesic, shallow Typic Torriorthents) series are associated with the finer textured portions of the Morrison formation and shale badland areas. They have exchangeable sodium percentages (ESP) ranging from 15 to 50% and subsoil pH >9.0. Bributte

soils occupy complex hillslopes and ridges, usually within or adjacent to the Brushy Basin member, whereas Hadden soils occur on slopes and terraces between structural bench remnants within the Salt Wash member, and on gently sloping hills and small alluvial plains where the Brushy Basin and Salt Wash members of the Morrison formation converge. Casmos soils (loamy, mixed, superactive, calcareous, mesic Lithic Torriorthents), which have lower pH and lower ESP, occur on steep hillslopes and ridges associated with sandstone outcrops of structural bench remnants of the Salt Wash member of the Morrison formation and Dakota sandstone remnants.

Both gypsic and natric soils commonly support sparse vegetation covers, often <10% cover, consisting of galleta grass [*Hilaria jamesii* (Torrey) Bentham], Indian rice grass (*Stipa hymenoides* Roemer & Schultes), and shadscale [*Atriplex confertifolia* (Torrey & Fremont) S. Watson]. Mormon tea (*Ephedra* spp.) is more common on gypsic soils, whereas saltbushes (*Atriplex* spp.) are more common on natric soils. (All plant taxonomy is according to Welsh et al. [2003].) Well-developed biological soil crusts occur on soils rich in gypsum in near-surface soil horizons.

Soils that are neither gypsic nor natric occur on many different geologic formations and topographic positions throughout the study area. They support a wide variety of plant species, although vegetation cover remains sparse. These soils include Entisols and Aridisols of the Farb (loamy, mixed, superactive, calcareous, mesic Lithic Torriorthents), Moenkopie (loamy, mixed, superactive, calcareous, mesic Lithic Torriorthents), Moffat (coarse-loamy, mixed, superactive, mesic Typic Haplocalcids), Ravola (fine-silty, mixed, active, calcareous, mesic Typic Torrifluvents), Sandbench (sandy, mixed, mesic Typic Haplocalcids), Shalet (loamy, mixed, active, calcareous, mesic, shallow Typic Torriorthents), and Trook (coarse-loamy, mixed, superactive, mesic Typic Haplocalcids) series.

Landsat 7 ETM Data Processing and Analysis

Landsat 7 ETM imagery from Path 37, Row 33, acquired 6 June 2000, was obtained from Utah State University's Remote Sensing/Geographic Information Systems (RS/GIS) Laboratory, which was recently established as the Intermountain Region Digital Image Archive Center. The image had been geometrically corrected to a UTM Zone 12 north, NAD83/GRS1980 datum/spheroid projection. The image metadata reports a horizontal position accuracy of ±30 m. Landsat 7 ETM Bands 1 through 5 and 7 were analyzed with ERDAS Imagine image processing software (Leica Geosystems, 2002). The ETM image was subset to focus on the study area (Fig. 1).

All spectral bands were atmospherically adjusted using the cosine theta (COST) method with dark object subtraction (Chavez, 1996), which is a relatively simple and image-based alternative to more costly and complex atmospheric correction methods. With information on gains and biases obtained from the image's header file, digital numbers (DN) from the satellite were converted to reflectance percentage and path radiance was corrected by dark object subtraction. The script (Image Standardization Script no. 2) was downloaded from Utah State University's RS/GIS Laboratory (www.gis.usu.edu/imgstandard.html; verified 14 Sept. 2006) and the model was executed using Imagine. Dark object values were chosen by locating multiple deep shadow areas within the scene for visible light (Bands 1, 2, and 3) and water bodies for NIR (Band 5) and SWIR (Bands 5 and 7) and recording the DN value for each band. Sixteen dark-object DN values from the scene for each band were averaged to arrive at the dark-object DN used for each band in the COST correction model; average dark-object DN was checked against the low-end slope break for the DN histogram for each band.

Because the Landsat 7 ETM image may be visually analyzed using only three bands at one time (assigned to red, green, and blue), we determined the three-band combination that had the greatest amount of variance within the scene by calculating the OIF (Jensen, 2005). The OIF ranked all possible three-band combinations of Landsat 7 ETM Bands 1 through 5 and 7 for a scene using the following equation:

$$\text{OIF} = \Sigma s_k / \Sigma \text{ Abs}(r_j)$$

where s is the standard deviation for Band k, and Abs(r_j) is the absolute value of the correlation coefficient between any two of the three bands being evaluated. The band combination with the highest OIF has the highest variance and lowest duplication for the scene, and thus contains the greatest amount of information about the scene. The highest OIF for the entire study area was with Bands 1, 5, and 7, which has been used to distinguish arid landforms and gypsum crust (Al-Juaidi et al., 2003). The second-highest OIF was with Bands 4, 5, and 7. We chose to visually analyze the scene with these two most optimal band combinations: Bands 7, 5, and 1 assigned to red, green, and blue, respectively; and Bands 4, 5, and 7 assigned to red, green, and blue, respectively. The Image Drape feature in Imagine was used to visualize the landscape in three dimensions, guided by the OIF. An example of Imagine's image drape feature comparing visible light to the OIF 7–5–1 band combination assigned to red, green, and blue, respectively, which clearly distinguishes surficially gypsiferous soil from siltstone rock outcrop, is shown in Fig. 2.

Developing Normalized Difference Ratio Models for Predicting Gypsic and Natric Soil Areas

Locations within the study area that were visually estimated during field observation to have ≥50% by weight gypsum within a few centimeters of the soil surface were selected as training sites for areas with gypsic soils. These areas were dominated by gypsum-rich soils of the Goblin and Mussentuchit series formed from the Carmel formation. Landsat spectral plots of gypsic soils revealed much higher reflectance in SWIR Band 5 than SWIR Band 7 (Fig. 3A). The spectral difference in the regions of Band 5 vs. 7 is similar to broad spectral patterns indicated by numerous spectral plots for gypsum viewable at the USGS Digital Spectral Library (speclab.cr.usgs.gov/spectral.lib04/spectral-lib.desc+plots.html; verified 14 Sept. 2006) (Clark et al., 1993). In contrast to the USGS plots for gypsum, visible light reflectance values for the training areas rich in pedogenic gypsum near the soil surface are low, which is probably caused by high surface roughness and the presence of dark biological soil crusts.

Locations within the study that were determined by field observation to be dominated by sodic soils of the Hadden and Bributte series were selected as training sites for areas with natric soils. Landsat spectral plots of natric soil areas revealed higher reflectance in SWIR Band 5 than NIR Band 4 (Fig. 3B). The spectral absorption in the NIR is characteristic of Fe-bearing minerals. The clay-rich parent material of natric soils appeared to be high in Fe-rich smectite (e.g., Morrison formation), and natric soil areas were often associated with areas of rock outcrop and rock fragments covered with a well-developed, Fe-rich varnish. The spectral difference in the regions of Band 5 vs. 4 is similar to broad spectral patterns indicated by numerous spectral plots for Fe-bearing minerals (e.g., nontronite and hematite) viewable at the USGS Digital Spectral Library (Clark et al., 1993).

We developed two normalized difference ratio models of spectral data to exploit the differences in reflectance between spectral bands for areas with gypsic and natric soils. Normalized difference ratio models, similar in form to the commonly used NDVI (Rouse et al., 1973), were created to capture spectral differences between two bands while being relatively unaffected by variation in solar illumination caused by

topography, and use atmospherically adjusted reflectance values. The basis for the gypsic index is a normalized difference ratio:

$$(\text{Band 5} - \text{Band 7})/(\text{Band 5} + \text{Band 7}).$$

Similarly, the basis for the natric index is

$$(\text{Band 5} - \text{Band 4})/(\text{Band 5} + \text{Band 4}).$$

In each case, high normalized difference ratio values indicate high probability that the respective soil type is present on the land surface. The models were created in Imagine's Model Maker, archived, and executed using Imagine image processing software.

For both gypsic and natric models, threshold normalized difference ratio values were determined iteratively by trial and error. The models were executed multiple times and compared to areas known to contain gypsic or natric soils. Final threshold values for each model were selected to include areas with gypsic or natric soils and exclude areas with neither gypsic nor natric soils. Threshold ratio values >0.11 were considered indicative of areas dominated by gypsic soils, whereas threshold values >0.19 were considered indicative of areas dominated by natric soils. A conditional statement, along with a focal majority algorithm and low pass filter, were used to exclude normalized difference ratio values that were lower than the threshold values. Excluded values were given a value of 0 while included values were given a value of 1. Clump and sieve functions were used to eliminate single, scattered pixels, thus creating output layers for each model indicating areas with relatively high probability of the occurrence of gypsic or natric soils on the landscape.

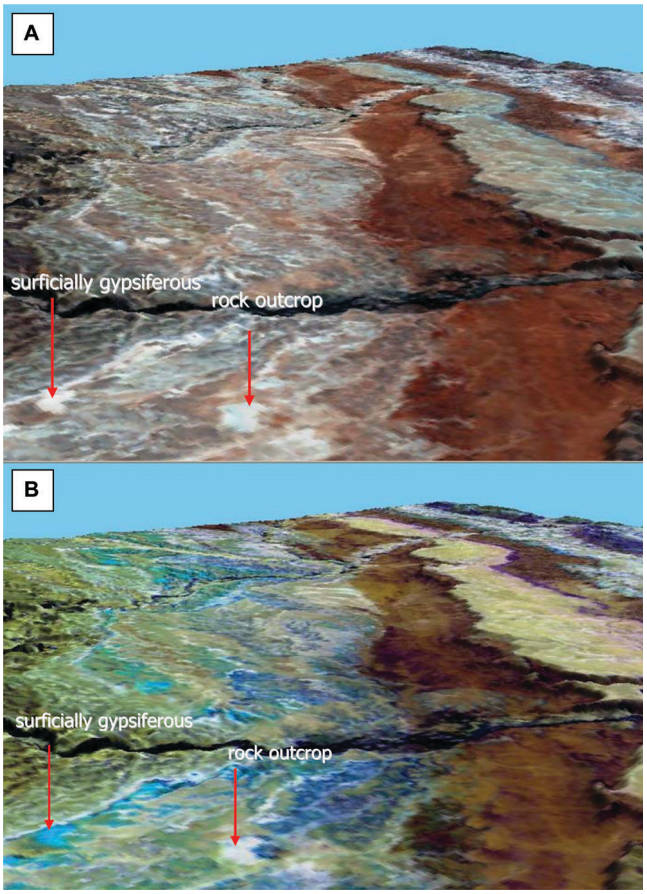

Fig. 2. Landsat 7 ETM image draped over the digital elevation model, with a landscape perspective looking southwest, to illustrate the optimum index factor for determining optimal band combinations for visually exploring the scene: (A) visible light Bands 3, 2, and 1 assigned to red, green, and blue, respectively, showing little differentiation between siltstone rock outcrop and surficially gypsiferous soils (both appear white); (B) optimal band combination 7, 5, and 1 assigned to red, green, and blue, respectively, distinctly differentiating between siltstone rock outcrop (appears white) and surficially gypsiferous soil (appears turquoise blue).

Accuracy Assessment

Two watersheds contributing to the upper San Rafael River that had limited road access were delineated to assess the accuracy of the normalized difference ratio models for predicting the occurrence of areas with gypsic and natric soils. One watershed that drained from southwest to northeast into the Fuller Bottom alluvial area was dominated by Carmel and Entrada formations and was predicted by the gypsic model to have fairly extensive areas with gypsic soils (Fuller Bottom watershed, Fig. 4). A second watershed that drained northeast to southwest into the Hambrick Bottom alluvial area was dominated by the Morrison formation and predicted to have fairly extensive areas of natric soils (Hambrick Bottom watershed, Fig. 5).

Digital elevation models (DEMs) with a spatial resolution of 10 m were obtained from the State of Utah's Automated Geographic Reference Center (UTM Zone 12 projection and NAD 83 datum) and analyzed using ESRI ArcMap and ArcInfo (Environmental Systems Research Institute, 2003). The DEMs for the Hadden Holes, Buckhorn Wash, Horn Silver Gulch, and Sid's Mountain 7.5′ quadrangles were mosaicked into a seamless DEM for the entire study area. The TauDEM extension for ArcMap (Tarboton, 2004) was used to delineate the Fuller Bottom and Hambrick

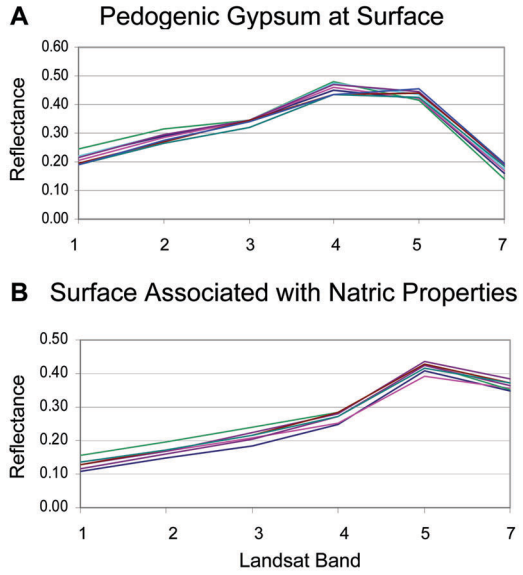

Fig. 3. Landsat spectral band profiles of (A) seven areas dominated by soils identified in the field to have ≥50% pedogenic gypsum within a few centimeters of the soil surface—note the peak in shortwave infrared (SWIR) Band 5 (1.55–1.75 µm) and absorption feature in SWIR Band 7 (2.08–2.35 µm); and (B) seven areas dominated by soils identified in the field to have natric properties—note the peak in SWIR Band 5 (1.55–1.75 µm) compared with relatively low reflectance values (absorption features) in near-infrared Band 4 (0.775–0.900 µm).

Bottom watersheds. The TauDEM first identified and filled elevational sinks. Flow directions and flow paths were then calculated and watershed boundaries were determined. The mosaicked DEM for the entire study area was then clipped by a boundary layer derived from the watershed delineations for Fuller Bottom and Hambrick Bottom.

A formal accuracy assessment involving field verification of the gypsic and natric model output maps was performed in the Fuller Bottom and Hambrick Bottom watersheds following the procedures of Congalton and Green (1999). To develop a valid accuracy assessment matrix, the number of field assessment sites was determined according to

$$N = B\pi_i(1 - \pi_i)/b_i^2$$

where N is the number of samples (field assessment sites), B is determined from a chi-square table with 1 degree of freedom and $1 - \alpha/k$ where k represents the number of categories classified and α represents the chance of rejecting the classification when it is actually correct, π_i is the largest expected percentage of any one category, and b_i is the desired precision or chance that, because of sample selection errors, the final product will have an accuracy less than desired. Each of the field assessment sites would be classified as either gypsic, natric, or neither gypsic nor natric ($k = 3$). Considering the difficulty of access and time constraints, a precision value (b_i) of 18%, a confidence level (α) of 95%, and a largest percentage expected of any one class (natric, gypsic, or not natric or gypsic, π_i) of 50% were chosen, resulting in a total of 93 field assessment sites.

Initially, randomly distributed accuracy assessment points were generated using ERDAS Imagine software, evenly stratified between areas predicted to have gypsic soils, natric soils, and neither gypsic nor natric soils; however, the extreme ruggedness of terrain and limited road access greatly increased the time required to complete the accuracy assessment using all randomly generated locations. To hasten the process, areas predicted to have gypsic or natric soils were identified on output maps. The coordinates of these areas were identified on the map and navigated to by foot using a hand-held global positioning system (GPS) unit. Within what was mapped as an area with gypsic or natric soils on the map, a representative site (minimum 30- by 30-m area) was chosen for assessment. We then navigated to a site clearly outside the gypsic or natric polygon to assess soils and landscapes predicted to be neither gypsic or natric. Multiple traverses were made across each watershed, with ≥150 m between each assessment site, until a total of 93 assessment sites were visited (see Fig. 4 and 5). There were 39 assessment points in Fuller Bottom watershed and 54 in Hambrick Bottom watershed.

A rule set was established to determine the correct classification of the soil–landscape unit observed in the field at each assessment site. If the assessment site was dominantly covered either in soil that contained at least 50% pedogenic gypsum masses within a few centimeters of the surface (e.g., Goblin series) or had gypsum-rich soil associated with gypsum-bearing rock outcrop, the site was classified as gypsic (e.g., Fig. 6). If the soil occurring at the designated assessment site fell within the Hadden or Bributte series or the landscape was typical for map units containing Hadden or Bributte components and associated with shale badlands, the site was classified as natric. At each assessment site, the soil series (e.g., Goblin) or map unit component (e.g., gypsum rock outcrop) was determined, photos were taken of soil exposed in a pit and the surrounding landscape, photo numbers were recorded, and spatial coordinates were acquired using the GPS. The GPS points were downloaded and converted to point coverages in ArcGIS for display (see Fig. 4 and 5).

RESULTS

The two normalized difference ratio models predicted the occurrence of gypsic and natric soils throughout the study area (Fig. 1). The most extensive areas of gypsic soils were predicted to occur most closely associated with the gypsum-rich Carmel formation on the southeastern flank of the study area. A few, smaller gypsic soil areas were predicted to occur where the Tununk member of the Mancos shale is adjacent to the Brushy Basin member of the Morrison formation, and around the margins of the Salt Wash member of the Morrison formation. The most extensive areas of natric soils were predicted to occur on the Salt Wash member of the Morrison formation and the Tununk member of the Mancos formation. While we expected to see these general soil–parent material patterns, the natric soils predicted to occur on the Curtis formation (mainly sandstone) were not expected.

The output map of the normalized difference ratio model predicting areas with gypsic soils in the Fuller Bottom watershed is shown in Fig. 4, underlain by the Landsat 7 ETM image (OIF Bands 1, 5, and 7). The accuracy assessment showed that the prediction of gypsic soil areas by the normalized difference ratio (Bands 5 and 7) model was highly accurate (Table 2). Of the 21 sites predicted by the map to be gypsic, 21 were confirmed in the field (e.g., Fig. 6). Of the 24 total sites observed in the field to be gypsic, 21 were predicted by the map to be gypsic. Using the terminology of Congalton and Green (1999), the user's accuracy was 100%, whereas the producer's accuracy was 87%. (While the user found 100% of the gypsic soil area sites predicted by the map to be gypsic, only 87% of the total sites determined in the field to be gypsic were correctly modeled as gypsic.)

The output map of the normalized difference ratio model predicting areas with natric soils in the Hambrick Bottom watershed is shown in Fig. 5, underlain by the Landsat 7 ETM image (OIF Bands 4, 5, and 7). Of the 17 sites predicted by the map as natric, 14 were observed to be natric (e.g., Fig. 7), resulting in a user's accuracy of 82%. Only 14 of the 27 sites observed in the field to be natric were predicted by the map to be natric, however, resulting in a producer's accuracy of 52%.

None of the soils predicted to be gypsic were observed to be natric, and none of the soils predicted to be natric were observed to be gypsic, indicating that these soil areas have very different spectral properties. The overall accuracy of this modeling and mapping effort in these two watersheds was about 80% (Table 2).

Table 2. Error matrix generated from the accuracy assessment of the natric and gypsic indices. Model reference classes were those shown on the output maps (predicted class). Field reference classes were determined by the field observation (observed classes).

Model reference	Accuracy assessment sites: Field reference			Total predicted	Producer's accuracy		User's accuracy	
	Gypsic	Natric	Neither		Ratio	Percentage	Ratio	Percentage
Gypsic	21	0	0	21	21/24	87.5	21/21	100
Natric	0	14	3	17	14/27	51.9	14/17	82.4
Neither	3	13	39	55	39/42	92.9	39/55	70.9
Total observed	24	27	42	93				
Overall accuracy = 74/93 = 79.6%								

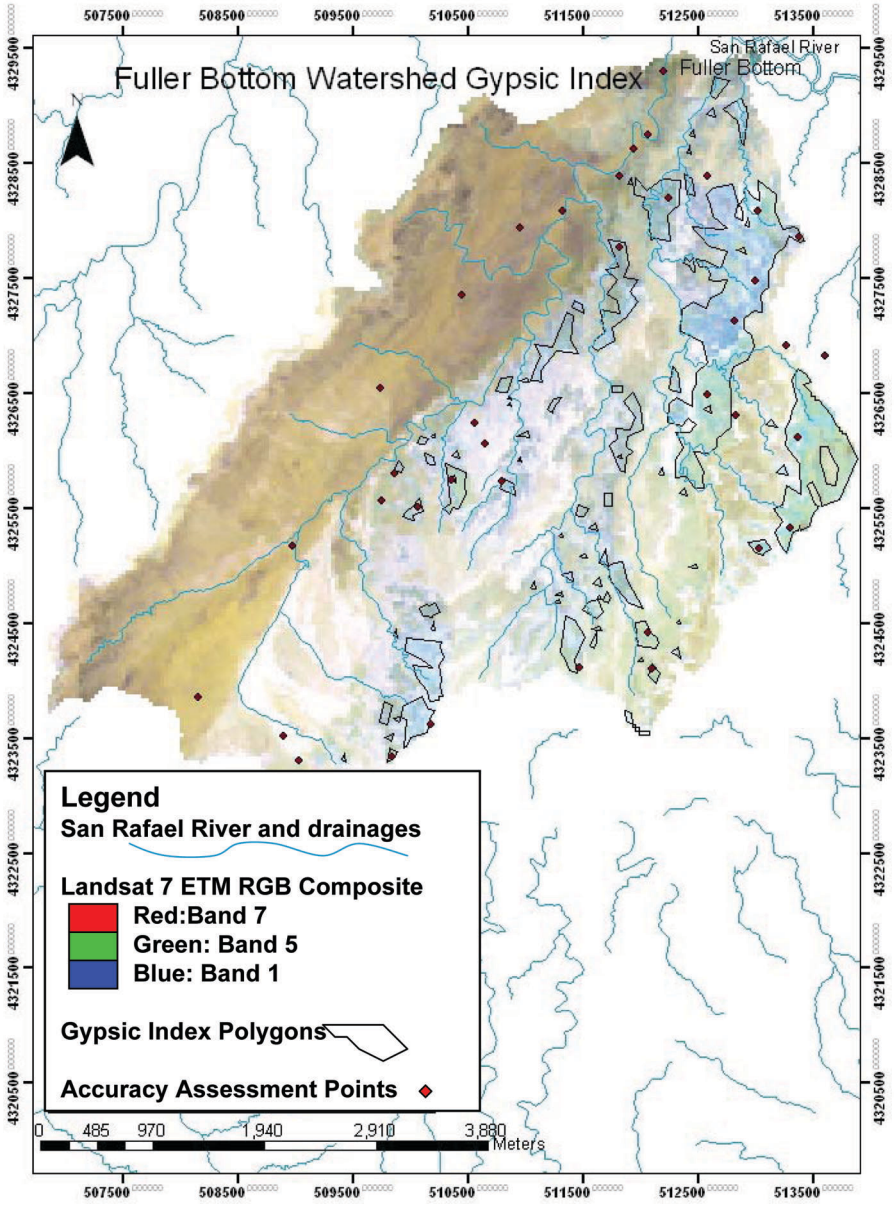

Fig. 4. Output of the gypsic index model within Fuller Bottom watershed, underlain by hydrology coverage and optimum index factor Landsat 7 ETM Bands 1, 5, and 7. Accuracy assessment sites inside and outside of gypsic pixel clusters (polygons) are shown. Carmel formation (white to pale) dominates the eastern flank, whereas Entrada formation (tan) dominates the western flank of the watershed.

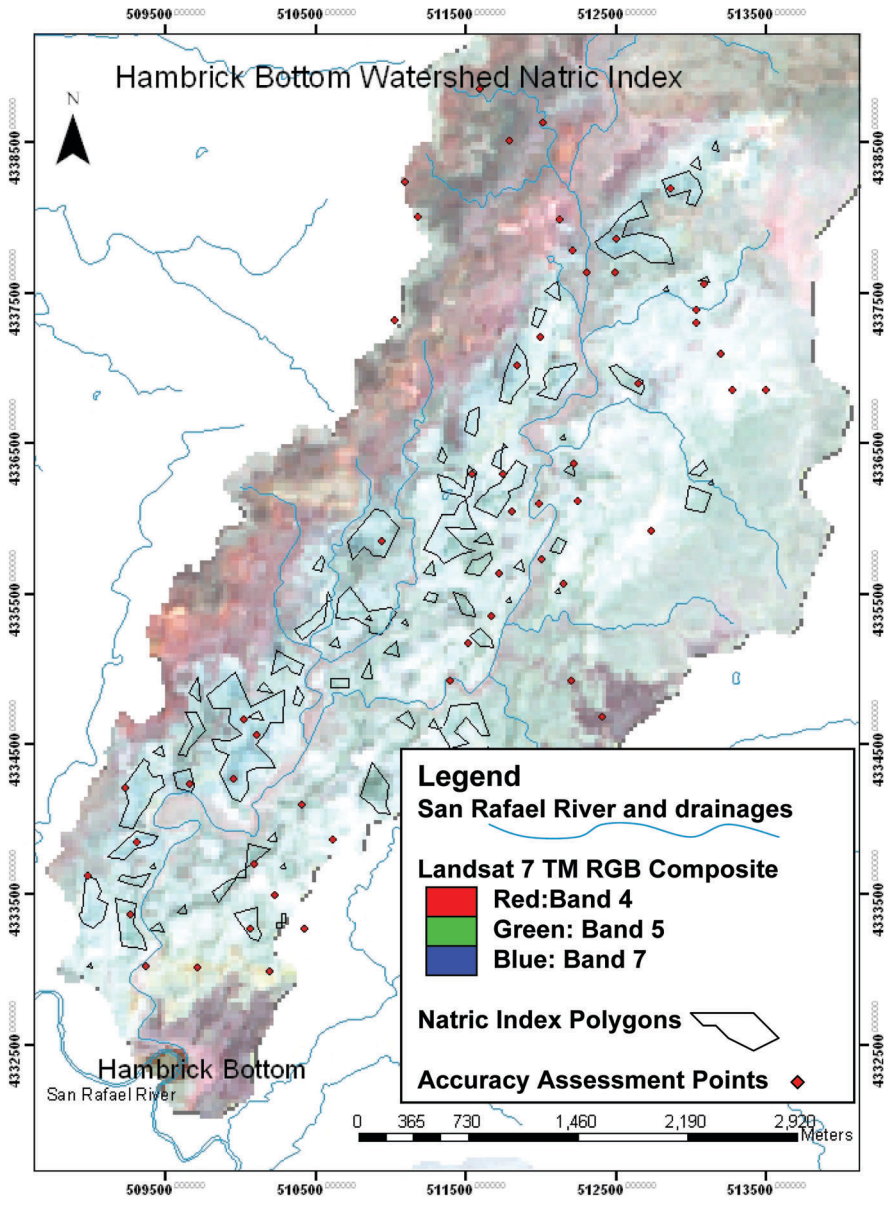

Fig. 5. Output of natric index model within Hambrick Bottom watershed, underlain by hydrology coverage and optimum index factor Landsat 7 ETM Bands 4, 5, and 7. Accuracy assessment points inside and outside natric index pixel clusters (polygons) are also shown. Morrison formation (white, gray-green, and rose) dominates the watershed, with some Cedar Mountain formation (pale tan) in the north.

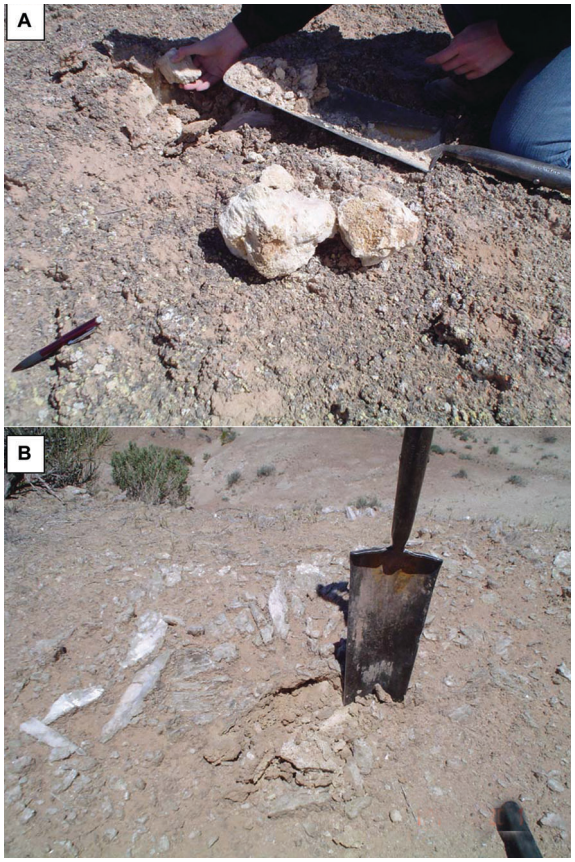

Fig. 6. Accuracy assessment sites predicted by normalized difference ratio (Bands 5 and 7) model to be gypsic and observed in the field to be gypsic: (A) Goblin soil series (loamy, gypsic, mesic, shallow Typic Torriorthent) with large masses of pedogenic gypsum a few centimeters below the soil surface, which is covered by a well-developed biological soil crust; (B) gypsum rock outcrop commonly associated with soils of the Goblin series.

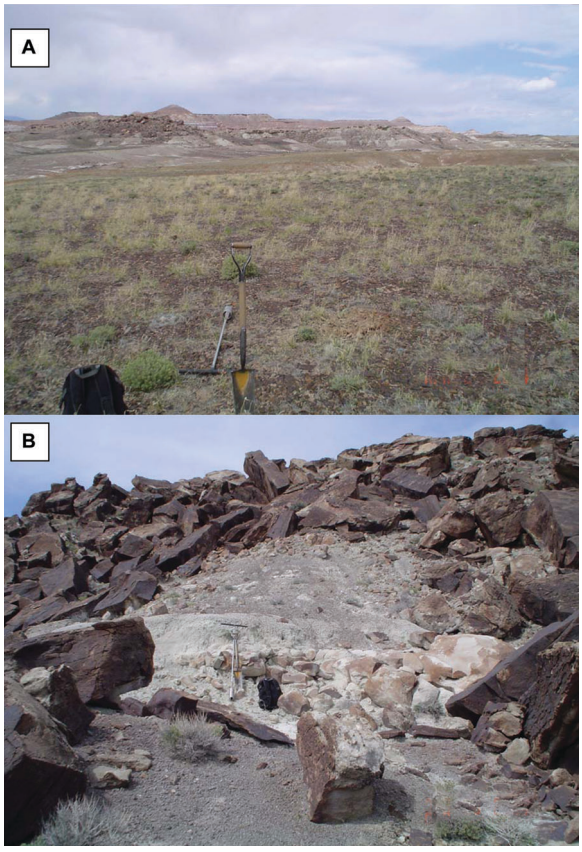

Fig. 7. Accuracy assessment sites predicted by normalized difference ratio (Bands 5 and 4) model to be natric and observed in the field to be natric: (A) darkly varnished sandstone cobbles and gravels (foreground) at the surface of the Hadden series (fine-loamy, mixed, superactive, mesic Typic Natrargid); (B) darkly varnished sandstone underlain by sodic shale parent material.

DISCUSSION

The model predicting gypsic soil areas was highly accurate, but the producer's accuracy was lower than the user's accuracy. This may have been caused in part by the assignment of "not gypsic or natric" accuracy assessment points that were too close to the mapped boundary of a gypsic soil area. For example, two of the three assessment sites observed in the field to be gypsic that were not mapped as gypsic were <30 m from the edge of a mapped gypsic soil area, which is less than the ±30-m horizontal position accuracy of the Landsat scene. Future accuracy assessment sites located ≥30 m from mapped boundaries may alleviate such problems.

Field observations during the accuracy assessment indicated that the normalized difference ratio (Bands 5 and 7) model was able to map areas that have gypsum within a few centimeters of the soil surface, regardless of the presence or absence of a biological soil crust. While some areas mapped as gypsic had soils or gypsum rock outcrop with little to no biological soil crust (e.g., Fig. 6B), other soils co-occurred with well-developed biological soil crusts (e.g., Fig. 6A), indicating that the model is responding primarily to the spectral reflectance of the gypsum. The model would have difficulties, however, mapping gypsiferous soils that have undergone more extensive pedogenesis to translocate gypsum from near-surface to subsurface horizons (e.g., some pedons of the Robroost series), and may require additional site-specific modeling (e.g., Farifteh et al., 2006).

While most (82%) of the areas predicted by the normalized difference ratio (Bands 5 and 4) model to have natric soil were confirmed in the field, only 52% of the sites observed in the field to have natric soils were predicted to be natric. Therefore, natric soil areas are probably more challenging to detect spectrally than gypsic soils. While gypsic soil areas appeared to have distinct spectral reflectances produced by gypsum at or near the soil surface, natric soil areas do not appear to have a "sodic" spectral signature. Natric soil areas primarily co-occurred with Fe-bearing minerals, such as that contained in darkly varnished sandstone rocks. In fact, most of the natric soil training sites included areas with darkly varnished sandstone outcrops. The 13 assessment sites that were predicted by the model as "neither" but were determined in the field to be natric soil areas did not exhibit a significant amount of darkly varnished sandstone outcrops or rock fragments at the surface. All 13 of these sites had different colors when viewed in the Landsat 7 ETM scene using OIF Bands 4, 5, and 7 than the areas correctly predicted to be natric (Fig. 5), probably indicating different surface mineralogy. Spectral analysis of additional training sites may provide insight on how to improve the modeling of a wider range of natric map units in the study area. Focusing the application of the natric model on areas derived from known Na-producing geologic formations may reduce overprediction of natric soils where Fe-bearing minerals at the soil surface do not co-occur with natric soils. For example, the high normalized difference ratio that

occurred on the Curtis formation was probably caused by the relatively high Fe content of a blue-tinted layer of sandstone exposed at the surface and not by natric soils (Fig. 1).

Normalized difference ratio models show promise for the digital mapping of soil areas associated with uniquely distinct differences in two Landsat spectral bands. Exploration of a Landsat scene using the highest OIF band combinations can guide the user to the spectral bands that may be diagnostic for particular land surface features within a study area. Once possible band differences are recognized, normalized difference ratio models are relatively simple to construct and execute for a Landsat scene using ERDAS Imagine or other image processing software. We speculate that the normalized difference band ratio using Bands 5 and 7 to map high concentrations of gypsum (e.g., ≥50%) near the soil surface can be transferred to other areas, such as throughout the arid Colorado Plateau; however, the threshold value may have to be adjusted to the specific study area. We encourage the creative exploration and analysis of Landsat data and the development of normalized index ratio models and specific thresholds where they may be applicable. For example, Bodily (2005) developed a normalized difference ratio model and threshold value using Landsat ETM Bands 5 and 2, coupled with a 10-m DEM-derived slope layer and a fractional vegetation cover derived from the NDVI, to map limestone rock outcrop components (overall accuracy 87%) for a soil survey update in northern Utah.

CONCLUSIONS

The gypsic normalized difference ratio model (Bands 5 and 7) was very useful in identifying gypsic soil areas of the study area. We expect that the gypsic model can be transferred to other areas, particularly in the arid Colorado Plateau, with possible adjustment of threshold values. Gypsic soil areas often co-occurred with well-developed biological soil crusts, but the crust did not appear to affect spectral classification of highly gypsiferous soils. The natric normalized difference ratio model (Bands 5 and 4) was a fair indicator of natric soil areas on the landscape. However, some natric soils areas were not spectrally modeled, and some areas with Fe-rich surface rocks did not have natric soils. Additional training sites may be needed to model the spectral diversity of natric areas in the study area. The relatively easy development and execution of normalized difference vegetation ratio models should facilitate their use in routine digital soil mapping and soil survey update activities.

ACKNOWLEDGMENTS

Funding was provided by the Colorado River Basin Salinity Control Forum, USDA-NRCS, and Utah Agricultural Experiment Station. We sincerely thank USDA-NRCS and Utah State University soil scientists for field assistance and discussions on conceptual models and digital data analysis, especially Leland Sasser and Suzann Kienast-Brown. This research was supported in part by the Utah Agricultural Experiment Station, Utah State Univ., Logan; approved as Journal Paper no. 7770.

REFERENCES

Al-Juaidi, F., A.C. Millington, and S.J. McLaren. 2003. Merged remotely sensed data for geomorphological investigations in deserts: Examples from central Saudi Arabia. Geogr. J. 169:117–130.

Baumgardner, M.F., L.F. Silva, L.L. Biehl, and E.R. Stoner. 1985. Reflectance properties of soils. Adv. Agron. 38:1–44.

Ben-Dor, E. 2002. Quantitative remote sensing of soil properties. Adv. Agron. 75:173–243.

Bodily, J.M. 2005. Developing a digital soil survey update protocol at the Golden Spike National Historical Site. M.S. thesis. Utah State Univ., Logan.

Brown, D.J., K.D. Shepherd, M.G. Walsh, M.D. Mays, and T.G. Reinsch. 2006. Global soil characterization with VNIR diffuse reflectance spectroscopy. Geoderma 132:273–290.

Chavez, P.S. 1996. Image-based atmospheric corrections—revisited and improved. Photogramm. Eng. Remote Sens. 62:1025–1036.

Clark, P.E., M.S. Seyfried, and B. Harris. 2001. Intermountain plant community classification using Landsat TM and SPOT HRV data. J. Range Manage. 54:152–160.

Clark, R.N., G.A. Swayze, A.J. Gallagher, T.V.V. King, and W.M. Calvin. 1993. The U.S. Geological Survey digital spectral library. Version 1: 0.2 to 3.0 microns. U.S. Geol. Surv. Open File Rep. 93–592.

Congalton, R.G., and K. Green. 1999. Assessing the accuracy of remotely sensed data: Principles and practices. CRC Press, Boca Raton, FL.

Dwivedi, R.S., K. Sreenivas, and K.V. Ramana. 1999. Inventory of salt-affected soils and waterlogged areas: A remote sensing approach. Int. J. Remote Sens. 20:1589–1599.

Environmental Systems Research Institute. 2003. ArcGIS 8.3. ESRI, Redlands, CA.

Farifteh, J., A. Farshad, and R.J. George. 2006. Assessing salt-affected soils using remote sensing, solute modelling, and geophysics. Geoderma 130:191–206.

Fernandez-Buces, N., C. Siebe, S. Cram, and J.L. Palacio. 2006. Mapping soil salinity using a combined spectral response index for bare soil and vegetation: A case study in the former Lake Texcoco, Mexico. J. Arid Environ. 65:644–667.

Fillmore, R. 2000. The geology of the parks, monuments, and wildlands of southern Utah. Univ. of Utah Press, Salt Lake City.

Jensen, J.R. 2005. Introductory digital image processing. 3rd ed. Pearson Prentice Hall, Saddle River, NJ.

Jensen, E.H., and J.W. Borchert. 1988. Soil survey of Carbon area, Utah. U.S. Gov. Print. Office, Washington, DC.

Kienast-Brown, S., and J.L. Boettinger. 2006. Land cover classification from Landsat imagery for mapping dynamic wet and saline soils. p. 241–251. *In* P. Lagcherie et al. (ed.) Digital soil mapping: An introductory perspective. Dev. Soil Sci. 31. Elsevier, Amsterdam.

Leica Geosystems. 2002. ERDAS Imagine version 8.6. Leica Geosystems, Atlanta, GA.

Lillesand, T.M., and R.W. Kiefer. 2000. Remote sensing and image interpretation. John Wiley & Sons, New York.

Masoud, A.A., and K. Koike. 2006. Arid land salinization detected by remotely-sensed landcover changes: A case study in the Siwa region, NW Egypt. J. Arid Environ. 66:151–167.

Metternicht, G., and J.A. Zinck. 1997. Spatial discrimination of salt- and sodium-affected soil surfaces. Int. J. Remote Sens. 18:2571–2586.

National Aeronautics and Space Administration. 2006. Landsat then and now. Available at landsat.gsfc.nasa.gov/about/ (last accessed 27 June 2006; verified 14 Sept. 2006).

Pankova, E.I., and D.I. Rukhovich. 1999. Monitoring of salinization of irrigated soils in arid regions by remote sensing methods. Eurasian Soil Sci. 32:225–235.

Ramsey, R.D., D. Wright, and C. McGinty. 2004. Evaluating the use of Landsat 30m Enhanced Thematic Mapper to monitor vegetation cover in shrub-steppe environments. Geocarto Int. 19:39–47.

Rao, B.R.M., T.R. Sankar, R.S. Dwivedi, S.S. Thammappa, and L. Venkataratnam. 1995. Spectral behaviour of salt-affected soils. Int. J. Remote Sens. 16:2125–2136.

Rouse, J.W., Jr., R.H. Hass, J.A. Schell, and D.W. Deering. 1973. Monitoring vegetation systems in the Great Plains with ERTS. p. 309–317. *In* Proc. ERTS Symp., 3rd, Washington, DC. 10–14 Dec. 1973. NASA SP-351. Natl. Aeronaut. Space Admin., Washington, DC.

Tarboton, D. 2004. Terrain analysis using digital elevation models (TauDEM). Available at hydrology.neng.usu.edu/taudem/ (last accessed 2 Feb. 2006; verified 14 Sept. 2006). Utah State Univ.,

Utah Department of Environmental Quality. 2004. Colorado River West Watershed Management Unit water quality assessment—2004 305(b). Available at www.waterquality.utah.gov/documents/coloradoriverwest2004bfact-01-10-05.pdf (last accessed 3 Feb. 2006; verified 14 Sept. 2006). Division of Water Quality, Salt Lake City.

Welsh, S.L., N.D. Atwood, S. Goodrich, and L.C. Higgins. 2003. A Utah flora. 3rd ed. Brigham Young Univ., Provo, UT.